Clays and Clay Minerals, Vol. 50, No. 6, 736–745, 2002.

FORMATION OF SEPIOLITE-PALYGORSKITE AND RELATED MINERALS FROM SOLUTION

REZAN BIRSOY*

Dokuz Eylül University, Engineering Faculty Geology Department, 35100 Bornova, İzmir, Turkey

Abstract—Most of the world's sepiolite-palygorskite precipitates in lacustrine and perimarine environments. Although these minerals can transform from precursor minerals, the most common formation mechanism involves crystallization from solution. In this study, equilibrium activity diagrams are calculated for sepiolite-palygorskite in the seven component system MgO-CaO-Al_2O_3-SiO_2-H_2O-CO_2-HCl, employing available thermodynamic data for related minerals, aqueous species and water. Stability fields are illustrated graphically on plots of $\log [a_{Mg^{2+}}/(a_{H^+})^2]$ *vs.* $\log[a_{H_4SiO_4}^o]$, using the activities for $\log[a_{Al^{3+}}/(a_{H^+})^3]$ defined by an arbitrarily chosen value and the approximate saturation limits of pyrophyllite + amorphous silica, kaolinite + amorphous silica, kaolinite + pyrophyllite, pyrophyllite + quartz and gibbsite. The formation of sepiolite-palygorskite from solution is more favored in the presence of amorphous silica than quartz. Lower aqueous aluminum activities favor the non-aluminum phases sepiolite and kerolite relative to the aluminum-containing phases palygorskite and saponite. The stability ranges of worldwide associations of magnesite and dolomite with sepiolite and palygorskite are also illustrated as a function of aluminum activity.

Key Words—Activity Diagrams, Clays, Kerolite, Palygorskite, Saponite, Sepiolite, Solution.

INTRODUCTION

The palygorskite-sepiolite group minerals have layer ribbon structures and can be classified as intermediates between the chain/ribbon structures of pyroxenes and amphiboles, and the layer structures of smectites (Velde, 1985; Jones and Galán, 1988). Palygorskite and sepiolite show diverse modes of occurrence and mineral genesis. Deposits of these minerals have been found in marine, transitional marine and continental-lacustrine environments, in continental soils, and in association with igneous rocks (Jones and Galán, 1988). A variety of processes, such as direct precipitation, alteration of volcanic ash, detrital transport, and transformation from smectite, Mg-carbonate and serpentinite have been suggested as formation mechanisms. Precipitation from solution is the most commonly suggested mechanism for the formation of palygorskite-sepiolite from various kinds of deposits (Esteoule-Choux, 1984; Isphording, 1984; Velde, 1985; Yeniyol and Öztunalı, 1985; Jones and Galán, 1988; Singer and Galán, 1984; Bozkaya and Yalçın, 1993; Chahi *et al.*, 1993; Ece and Çoban, 1990; Kadir and Baş, 1995; Yalçın and Bozkaya, 1995a,b).

Regardless of the particular mechanism, the solution chemistry with respect to Mg, silica, Al and pH will control sepiolite-palygorskite crystallization. The utilization of activity diagrams will constrain the possible models for natural mineral occurrences. Furthermore, instead of suggesting approximate values for effective variables, it will be much more satisfying to introduce certain numerical threshold values for pH, Mg, Si and Al activities that are difficult to establish experimentally. Although natural sepiolite-palygorskite occurrences are commonly associated with amorphous silica, associations with quartz (Leguey *et al.*, 1984), talc (Isphording, 1984), kerolite (Stoessell and Hay, 1978) and saponite (Galán and Castillo, 1984) occur as well. Talc, kerolite and saponite are compositionally similar minerals that superimpose on the same field in the Mg-Si activity diagrams. The present study demonstrates the chemical conditions required for the formation of sepiolite-palygorskite and related minerals with respect to aqueous activities of Al, Mg, Si and H. To be able to distinguish the various assemblages, diagrams were constructed by suppressing various combinations of saponite, kerolite, talc, quartz and amorphous silica. Furthermore, depending on the saturation limits of dolomite and magnesite in the system MgO-CaO-Al_2O_3-SiO_2-H_2O-CO_2-HCl, the possibility of the precipitation of sepiolite, palygorskite or other clay minerals was investigated.

* E-mail address of corresponding author:
rezan.birsoy@deu.edu.tr

METHODS

Thermodynamic data

The calculations of reliable activity diagrams requires internally consistent thermodynamic data. Thermodynamic data for most minerals have been tabulated (*e.g.* Robie *et al.*, 1978; Helgeson *et al.*, 1978; Wagnam *et al.*, 1982; Robie and Hemmingway, 1995). However, thermodynamic data for some of the silicates, especially clay minerals, are not available. In such cases, thermodynamic values must be calculated. For this purpose various methods are available to model the silicate minerals (Tardy and Garrels, 1974; Chen, 1975; Nriagu, 1975; Mattigod and Sposito, 1978;

Chermak and Rimstidt, 1989; Tardy and Duplay, 1992). In the present study, free energy of formation ($\Delta G^0_{f,\,298}$) values for the minerals and ionic species were obtained from Helgeson *et al.* (1978) and Stoessell (1988). Values for saponite, sepiolite, palygorskite and Mg-montmorillonite were calculated by applying the method developed by Nriagu (1975), who used $\Delta G^0_{f,\,298}$ of component hydroxides to estimate the $\Delta G^0_{f,\,298}$ value for any layer silicate. This method involves summing the $\Delta G^0_{f,\,298}$ of the component hydroxides and subtracting $\Delta G^0_{f,\,298}$ of liberated water and an empirical correction factor. For example, the $\Delta G^0_{f,\,298}$ for palygorskite is given by the expression (Nriagu, 1975):

$$\Delta G^0_{f,\,298}(\text{paly}) = \Sigma n_i \Delta G^0_{f,\,298}(\text{hydroxide}) - (\Sigma n_i z_i - 30)\ \Delta G^0_{f,\,298}(H_2O) - Q$$

where Q is an empirical parameter $[0.39(n_i z_i - 30)]$ based on the number of water molecules gained or released during reaction, where n_i is the reaction coefficient of the i-th hydroxide and z_i is the charge on the i-th cation. With reference to the above equation, the procedure can be illustrated with the structural formula of palygorskite as follows:

$$Mg_{2.84}Al_{1.8}Si_{7.73}O_{20}(OH)_2(OH_2)_4.4H_2O + 12\ H_2O = 2.84Mg(OH)_2 + 1.8Al(OH)_3 + 7.73Si(OH)_4$$

$$\Delta G^0_{f,\,298}(\text{paly}) = 2.84(-202.12) + 1.8(-274.2) + 7.73(-318.6) - 12(56.69) - 0.39(12) = -2854.780\ \text{kcal/mol} = -11944.32\ \text{kJ/mol}.$$

The stability limits of carbonates for both magnesite and dolomite, which contribute to the paragenetic factors that control the occurrences of sepiolite and palygorskite, are also considered. Because the most common clay minerals associated with sepiolite and palygorskite are smectites, Mg-saponite and Mg-montmorillonite are also included as paragenetic phases in the system. Free energies of all the phases used to calculate activity diagrams in this study are given in Table 1.

Groundwater data

Groundwater data were obtained from the literature in order to determine the change in composition of groundwater which flows through the deposit that contains sepiolite-palygorskite and related minerals, and to ascertain whether water is in equilibrium with any of those phases or not. Groundwater data from Amboseli, Kenya were used for this purpose (Stoessell and Hay, 1978). Only ground and spring waters with exactly the same sample number as those of Stoessell and Hay (1978) were used (Table 2). Concentrations given in Table 2 were converted to thermodynamic concentrations for these calculations. Ionic strength values are suitable for using the extended Debye-Hückel equation (Nordstrom and Munoz, 1985) to calculate activity coefficients. To calculate true $\log(a_{Al^{3+}})$, all Al-hydroxy species (Drever, 1997) were considered during calculation. All water data were also recalculated by VMINTEQ (Gustafsson 2001, 2002) and used on final diagrams.

Table 1. Minerals, formulae and free energies ($\Delta G^0_{f,\,298}$).

Mineral	Chemical formula	Free energy $\Delta G^0_{f,\,298}$ (kJ/mol)
Quartz	SiO_2	−856.239 [1]
Amorphous silica	SiO_2	−850.599 [1]
Magnesite	$MgCO_3$	−1027.866 [1]
Dolomite	$CaMg(CO_3)_2$	−2167.228 [1]
Calcite	$CaCO_3$	−1130.098 [1]
Brucite	$Mg(OH)_2$	−835.319 [1]
Enstatite	$MgSiO_3$	−1459.923 [1]
Forsterite	Mg_2SiO_4	−2056.704 [1]
Chrysotile	$Mg_3Si_2O_5(OH)_4$	−4037.020 [1]
Kerolite	$Mg_3Si_4O_{10}(OH)_2H_2O$	−5736.700 [2]
Talc	$Mg_3Si_4O_{10}(OH)_2$	−5523.667 [1]
Anthophyllite	$Mg_7Si_8O_{22}(OH)_2$	−11361.359 [1]
Antigorite	$Mg_{48}Si_{34}O_{85}(OH)_{62}$	−66140.755 [1]
Gibbsite	$Al(OH)_3$	−1157.486 [1]
Pyrophyllite	$Al_2Si_4O_{10}(OH)_2$	−5520.920 [1]
Kaolinite	$Al_2Si_2O_5(OH)_4$	−3789.089 [1]
Chlorite	$Mg_5Al_2Si_3O_{10}(OH)_8$	−8181.394 [1]
Ca-saponite	$Ca_{0.165}Mg_3Al_{0.33}Si_{3.67}O_{10}(OH)_2$	−5600.092 [3]
Mg-saponite	$Mg_{3.165}Al_{0.33}Si_{3.67}O_{10}(OH)_2$	−5591.740 [3]
Sepiolite	$Mg_4Si_6O_{15}(OH)_2(OH_2)_2.4H_2O$	−9259.192 [3]
Palygorskite	$Mg_{2.84}Al_{1.8}Si_{7.73}O_{20}(OH)_2(OH_2)_4.4H_2O$	−11944.316 [2]
Mg-montmorillonite	$Mg_{0.167}Al_{2.33}Si_{3.67}O_{10}(OH)_2$	−5350.499 [3]
Water	H_2O	−237.190 [1]

[1] Helgeson *et al.* (1978)
[2] Stoessell (1988)
[3] Present study (Nriagu, 1975)

https://doi.org/10.1346/000986002762090263 Published online by Cambridge University Press

Table 2. Amboseli spring- and groundwater chemical analyses in ppm (Stoessell and Hay, 1978).

Sample no	pH	SiO_2	Al^{3+}	Mg^{2+}	Ca^{2+}	Na^{+}	K^{+}	Cl^{-}	SO_4^{2-}	F^{-}	HCO_3+CO_3^{2-}
1	7.00	39.8	0.0034	4.10	5.75	17.6	7.4	2.40	1.2	0.33	1.36
6	8.15	56.5	0.0005	11.6	10.0	247.0	36.1	205.0	21.6	1.4	8.28
7	9.95	44.5	0.024	0.37	1.79	946.0	84.0	533.0	50.2	4.1	27.58
8	8.30	63.3	0.0056	11.7	11.9	93.8	6.7	14.7	7.0	0.65	4.83
9	9.85	43.4	0.067	0.31	8.10	2030.0	34.6	953.0	136.0	10.0	59.90
11	7.90	105.	0.0005	16.6	17.3	741.0	92.6	73.0	360.0	5.8	27.04
13	7.95	62.6	0.0091	15.1	22.2	25.1	5.7	2.3	2.4	0.34	3.31
14	6.95	56.5	0.0007	11.6	15.8	21.6	7.3	2.6	2.0	0.30	2.59
18	7.90	94.4	0.0031	28.8	22.8	84.5	13.1	39.6	15.8	0.70	5.65
19	9.90	27.0	0.034	1.52	2.80	391.0	44.6	155.0	20.1	2.8	13.78
20	7.80	107.	0.024	60.4	21.9	1010.0	114.0	127.0	580.0	3.5	36.53
21	8.25	45.8	0.020	12.1	7.40	60.9	12.0	4.5	4.0	1.8	3.79
22	7.20	49.6	0.0087	9.15	13.3	18.5	6.5	2.4	4.0	0.39	2.21
23	7.10	38.1	0.0110	7.33	10.8	8.8	2.5	1.4	1.8	0.14	1.46

Geological characteristics of Amboseli waters: 1, 13, 14, 20, 21, 22, 23 in basalts; 8, 18, 19 in dolomite; 6, 7, 9, 11 in clays and sepiolite deposits

Construction of the activity diagrams

The activity diagrams presented here comprise the seven-component system MgO-CaO-Al_2O_3-SiO_2-H_2O-CO_2-HCl. This system can be readily represented in two dimensions as a function of $\log[a_{H_4SiO_4}^{o}]$ and $\log[Mg^{2+}/(a_{H^+})^2]$ while holding the aqueous activities of Al, water and gaseous CO_2 constant. For example, the stability line between palygorskite and solution is represented by simple hydrolysis reaction:

$$Mg_{2.84}Al_{1.8}Si_{7.73}O_{20}(OH)_2(OH_2)_4.4H_2O + 11.08H^+ + 0.92H_2O = 2.84Mg^{2+} + 1.8Al^{3+} + 7.73H_4SiO_{4(aq)}$$

The equilibrium constant as a function of pressure and temperature can be calculated from thermodynamic data for the above reaction and is expressed at 1 bar pressure and 25ºC temperature holding the activity of water as unity for the present study:

$$\log K = 2.84\log[a_{Mg^{2+}}/(a_{H^+})^2] + 7.73\log[a_{H_4SiO_4}^{o}] + 1.8\log[a_{Al^{3+}}/(a_{H^+})^3]$$

$$\log[a_{Mg^{2+}}/(a_{H^+})^2] = -2.272\log[a_{H_4SiO_4}^{o}] + 0.634\log[a_{Al^{3+}}/(a_{H^+})^3] + \log K/2.84.$$

Similar equations written for all mineral phases and their combinations represent stability fields of the minerals under consideration. Components not shown on the graphs (for example, $\log[a_{Al^{3+}}/(a_{H^+})^3]$) were assigned as the activity ratio of a saturated paragenetic mineral or as an arbitrarily chosen value. In the case of Al activity, six different values were selected to illustrate the geometry of the stability fields of the phases, which may change depending on the activity of aluminum. The solubility of gibbsite was taken as the highest value for the activity of Al $\log[a_{Al^{3+}}/(a_{H^+})^3]$, followed by pyrophyllite + quartz, pyrophyllite + kaolinite, kaolinite + amorphous silica, pyrophyllite + amorphous silica and a lowest arbitrary value. The method of calculating activity diagrams has been described in detail elsewhere (Garrels and Christ, 1965; Bowers *et al.*, 1984). Because sepiolite-palygorskite is associated with calcite and dolomite, the solubilities of calcite and dolomite are also plotted as dashed lines.

Experimental studies on the stability of sepiolite have demonstrated that if the silica activity value is higher than quartz saturation in alkaline solutions, sepiolite precipitates (Wollast *et al.*, 1968; Christ *et al.*, 1973). The experimental study of Stoessell (1988) and field observations of Jones (1986) suggest that kerolite and talc are more stable than sepiolite for all activities of silica. This suggests that reaction kinetics determine which mineral precipitates in sedimentary conditions as in the case of opal and quartz (*i.e.* quartz is more stable than amorphous silica but amorphous silica is much more common in young marine sediments than quartz). Consequently, sepiolite associates with saponite and occasionally kerolite in natural occurrences but not with talc. Singer and Norrish (1974) and Christ *et al.* (1973) argued that the phase relations would be difficult to establish when minerals contain elements such as Al and Fe. This is because of the low solubility of alumina and the difficulty of controlling the oxidation potential of the system caused by Fe. Since talc contains no alumina, it is favored in alumina-free systems. For this reason, activity diagrams are calculated either by suppressing saponite and kerolite or talc and kerolite, or saponite and talc. In some deposits, amorphous silica predominates (Stoessell and Hay, 1978; Yalçin and Bozkaya, 1995) and in others, quartz (Long *et al.*, 1997) is present. Thus, activity diagrams suppressing either quartz or amorphous silica are to be calculated separately.

Because kerolite is present in addition to sepiolite at Amboseli Basin (Stoessell and Hay, 1978), groundwater data were plotted on the activity diagrams containing kerolite to see the expected diagenetic changes in the deposit.

https://doi.org/10.1346/000986002762090263 Published online by Cambridge University Press

RESULTS

A series of diagrams for seven-component systems are shown in Figures 1–5 by suppressing saponite + kerolite + quartz, talc + kerolite + amorphous silica, talc + kerolite + quartz, talc + saponite + quartz and talc + saponite + amorphous silica, respectively. Within each figure, six different Al activities are utilized in increasing order. In all diagrams, the solution is stable at low Mg^{2+} and silica activities.

In most field occurrences, amorphous silica is present instead of quartz, and the diagrams in Figure 1 were constructed by suppressing saponite, kerolite and quartz (Figure 1a–f). Talc occupies the field between dioctahedral and trioctahedral smectites with changing Al activities, and the stability of talc decreases with increasing Al activity, as expected. Minerals containing Al, however, increased their fields of stability.

Figure 2a–f illustrates the changes in the stability fields of quartz, Mg-montmorillonite, sepiolite, palygorskite, chlorite, saponite and chrysotile when talc + kerolite + amorphous silica are suppressed. The stability fields of quartz, sepiolite and chrysotile decrease, but those of Mg-montmorillonite and palygorskite increase with higher Al activities. Saponite appears when the Al

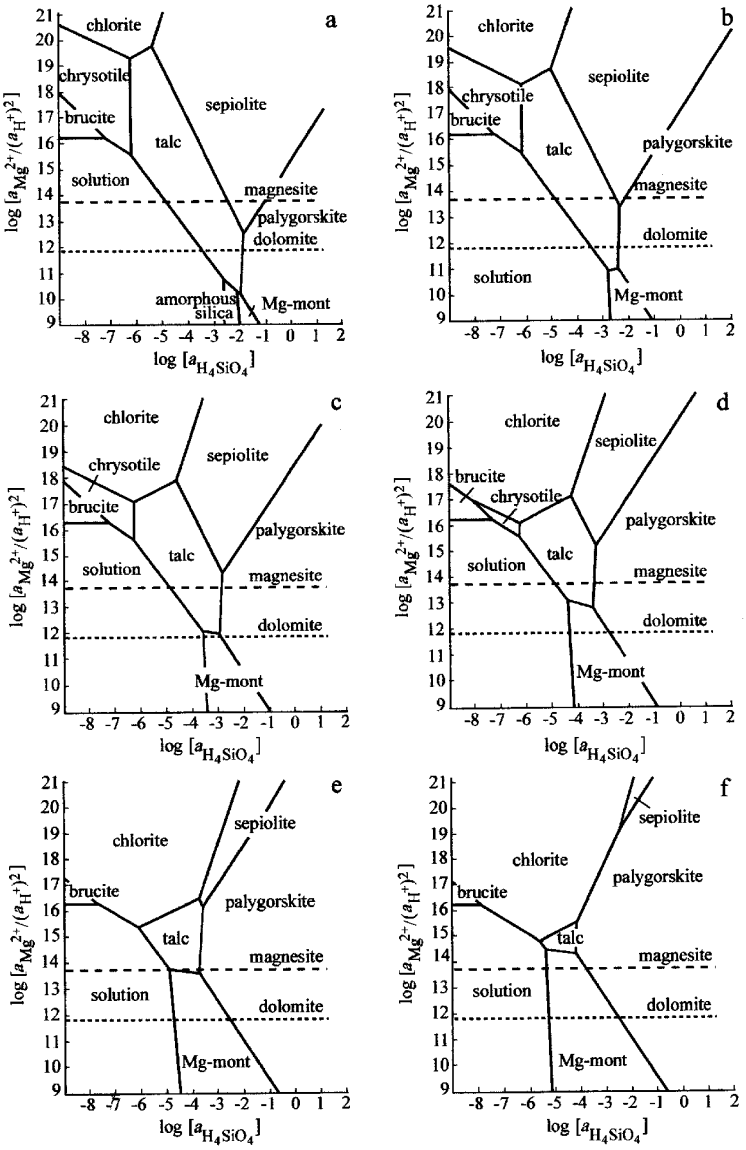

Figure 1. 25°C and 1 bar phase diagrams with $\log a_{H_2O} = 1$, $\log a_{CO_2} = -3.5$, and $\log[a_{Ca^{2+}}/(a_{H^+})^2] = 13.06$ and suppression of saponite, kerolite and quartz. The following $\log[a_{Al^{3+}}/(a_{H^+})^3]$ values are represented: (a) 4.5 (an arbitrary low value), (b) 5.5 (5.61 for pyrophyllite + amorphous silica saturation), (c) 6.5 (6.38 for kaolinite + amorphous silica saturation), (d) 7.5 (7.2 for kaolinite + pyrophyllite saturation), (e) 8.5 (8.35 for pyrophyllite + quartz saturation), (f) 9.2 (8.98 for gibbsite saturation). Saturation lines for magnesite and dolomite are indicated as dashed lines.

https://doi.org/10.1346/000986002762090263 Published online by Cambridge University Press

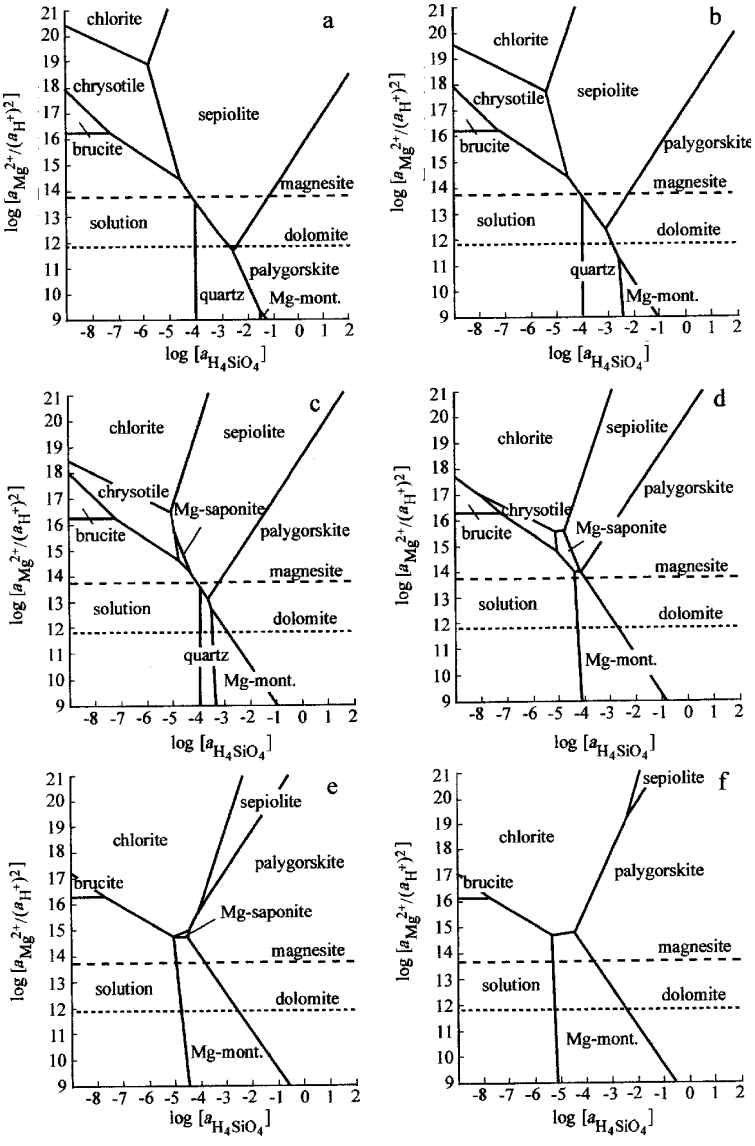

Figure 2. Same as Figure 1 but suppressed with respect to talc, kerolite and amorphous silica.

activity ratio $\log[a_{Al^{3+}}/(a_{H^+})^3]$ reaches 5.5. The saponite stability field reaches its maximum extent (Figure 2d) when the Al activity ratio $\log[a_{Al^{3+}}/(a_{H^+})^3]$ is 7.5. The stability field of saponite decreases when the Al activity ratio exceeds 7.5. When the Al saturation reaches gibbsite saturation, saponite has no stability field and sepiolite almost disappears (Figure 2f). Quartz is stable up to an Al activity ratio of 6.5. With increasing Al activities, palygorskite overtakes prior regimes of sepiolite stability.

For Figure 3a–f, talc + kerolite + quartz are suppressed, and amorphous silica appears as the stable phase. Amorphous silica naturally occupies a smaller stability field than quartz for the corresponding Al activities. The behavior of chlorite, chrysotile, Mg-montmorillonite, sepiolite, saponite and palygorskite are the same as when talc + kerolite + amorphous silica are suppressed (Figure 2), but the solution phase occupies a larger field with increasing Al activities.

Figures 4 and 5 are the counterparts of Figures 2 and 3 for activity diagrams of kerolite. Kerolite behavior is very similar to that of saponite except that kerolite occupies a greater stability field than saponite. When Figures 2 and 4, and 3 and 5 are compared, saponite is stable when values of $\log[a_{Al^{3+}}/(a_{H^+})^3]$ lie between 6.5 and 8.5 (Figures 2c–e and 3c–e), whereas kerolite is stable when these values are 7.5 and lower (Figure 4a–d).

Plotting the values of $\log[a_{Mg^{2+}}/(a_{H^+})^2]$ and $\log[a_{H_4SiO_4}]$ for the Amboseli waters on the activity diagrams resulted in a clustering in three groups, when $\log[a_{Al^{3+}}/(a_{H^+})^3]$ was not considered (Figures 4 and 5).

https://doi.org/10.1346/000986002762090263 Published online by Cambridge University Press

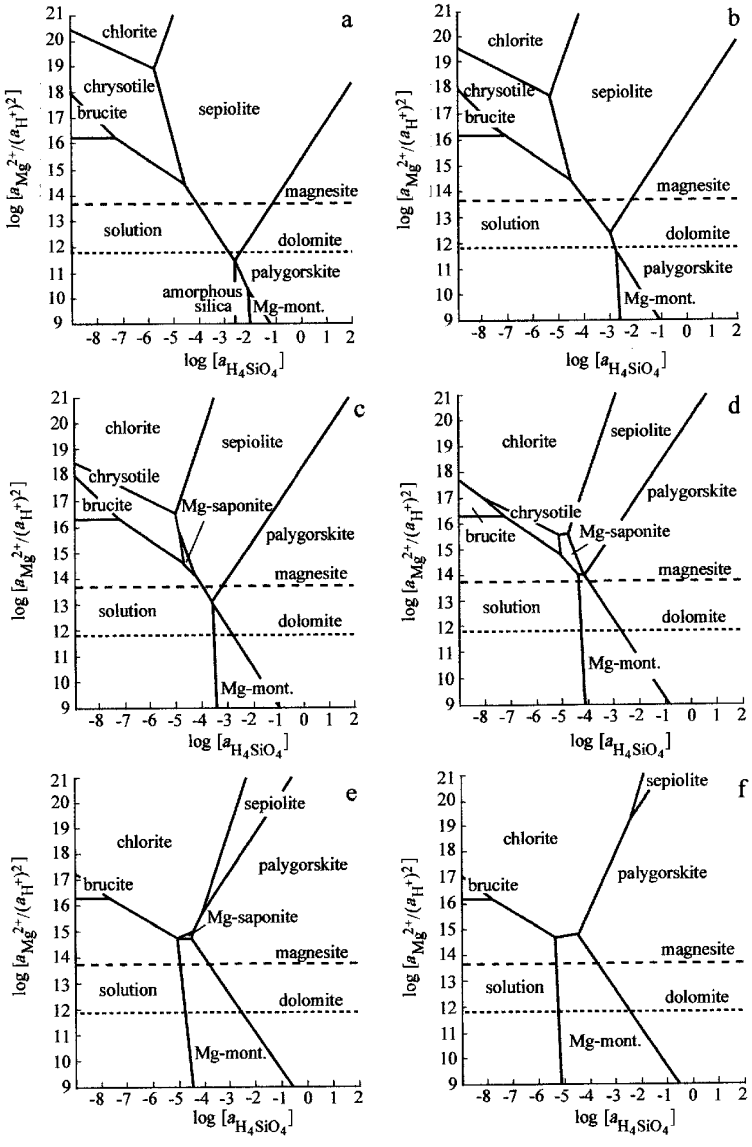

Figure 3. Same as Figure 1 but suppressed with respect to talc, kerolite and quartz.

The first group, which has a low log[$a_{Mg^{2+}}/(a_{H^+})^2$] value, includes the compositions of water samples labeled 1, 14, 22 and 23 in Table 2. The second group has moderate log[$a_{Mg^{2+}}/(a_{H^+})^2$] values, and includes water samples labeled 6, 8, 11, 13, 18, 20 and 21. The values for log[$a_{H_4SiO_4}$] are somewhat higher, and the system is supersaturated with respect to dolomite. The third cluster has the highest log[$a_{Mg^{2+}}/(a_{H^+})^2$] value, and includes samples labeled 7, 9 and 19, which are supersaturated with respect to dolomite and magnesite. When log[$a_{Al^{3+}}/(a_{H^+})^3$] values are considered, sample groups 13, 14, 20, 21 and 1, 22, 23, which have Al activity ratios in the range 8–9 (Figures 4e and 5e) and >9 (Figures 4f and 5f) respectively, are in the field of Mg-montmorillonite. Samples 8, 18 and 19 have a log[$a_{Al^{3+}}/(a_{H^+})^3$] value of ~7.5 (between 7 and 8), and are in the field of sepiolite and mostly palygorskite, and dolomite (Figures 4d and 5d). Samples 6, 7, 9 and 11 fall in the sepiolite and palygorskite fields with log[$a_{Al^{3+}}/(a_{H^+})^3$] values in the range 6–7 (Figures 4c and 5c). A decrease in log[$a_{Al^{3+}}/(a_{H^+})^3$] is consistent with the water flow direction and the composition of the rock through which water passes in the Amboseli basin (Figures 4c–d and 5c–d).

DISCUSSION AND CONCLUSIONS

Experimental studies and field occurrences demonstrate that for the formation of talc, kerolite, saponite and sepiolite, kinetic rather than thermodynamic factors control crystallization in the system MgO-CaO-SiO_2-Al_2O_3-H_2O-CO_2-HCl, at surface conditions. However, the activity diagrams calculated by suppressing talc also

https://doi.org/10.1346/000986002762090263 Published online by Cambridge University Press

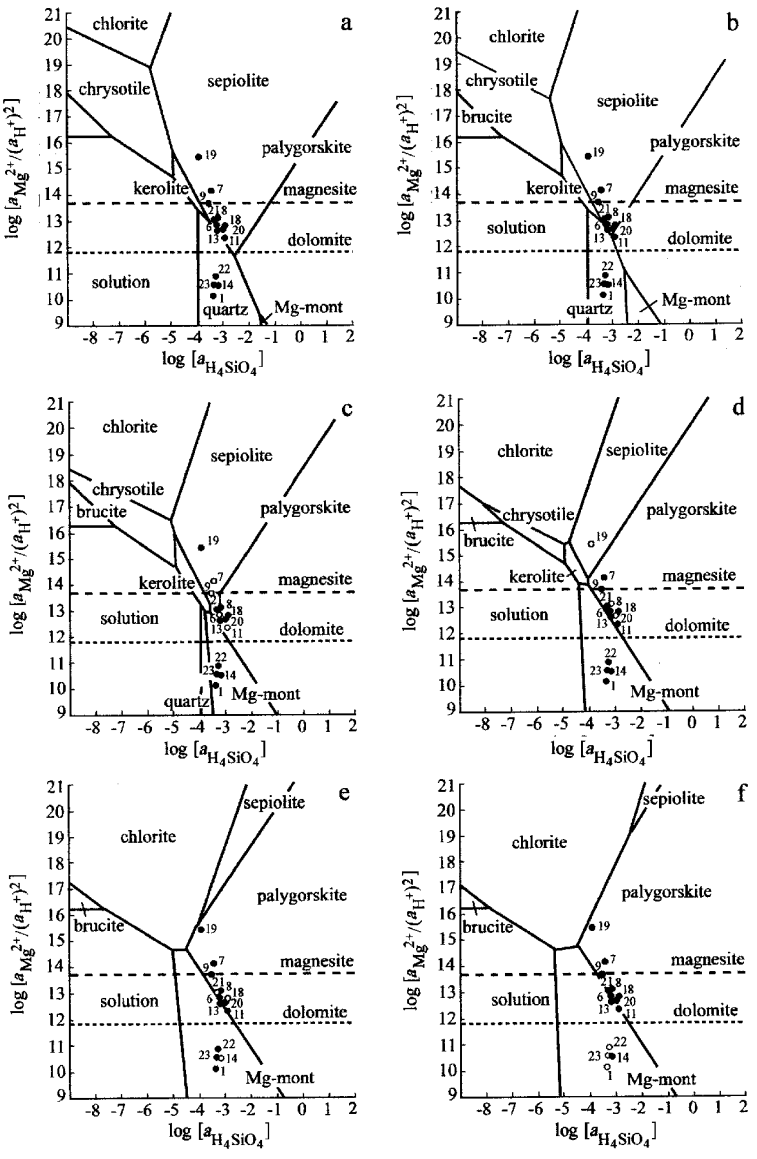

Figure 4. Same as Figure 1 but suppressed with respect to talc, saponite and amorphous silica. Symbol ○ indicates the water samples with the same $\log[a_{Al^{3+}}/(a_{H^+})^3]$ value as used in the activity diagram.

demonstrate that the direct precipitation of sepiolite and palygorskite from solution is favored by low values of $\log[a_{Al^{3+}}/(a_{H^+})^3]$. As seen in Figures 2a–c and 4a–c for example, palygorskite never forms from the solution in which quartz is the associated silica phase. In this case, palygorskite can form from dioctahedral smectite (low pH) and from quartz (Figures 2a–c and 4a–c), or from dioctahedral smectite (Figure 2d and 4d), or from dioctahedral and trioctahedral smectites (Figures 2e,f and 4e,f). In the case of sepiolite, however, when $\log[a_{Al^{3+}}/(a_{H^+})^3]$ is 7.5 or higher, it does not form from solution. At lower $\log[a_{Al^{3+}}/(a_{H^+})^3]$ values, the sepiolite can form both directly from solution and transformation from quartz (Figure 2a,b) or other minerals, when kerolite is the associated phase (Figure 4a,b). At an Al activity ratio $\log[a_{Al^{3+}}/(a_{H^+})^3]$ of 6.5, sepiolite forms from quartz, solution, trioctahedral smectites (saponite) and serpentine (chrysotile) (Figure 2c). Transformation from only trioctahedral smectites (saponite, chlorite) is possible at an Al activity ratio $\log[a_{Al^{3+}}/(a_{H^+})^3]$of 7.5 and above (Figures 2d–f and 4d–f). When the stabilities of magnesite and dolomite are taken into consideration, palygorskite is in equilibrium with both dolomite and magnesite when quartz is a stable phase. Palygorskite and dolomite and/or Mg-calcite, and sepiolite and magnesite, as paired assemblages, appear to be the most favored for natural occurrences. It is clearly observed that palygorskite and dolomite (or Mg-calcite), and sepiolite and magnesite are favored associates in calculated systems as well as in natural occurrences.

https://doi.org/10.1346/000986002762090263 Published online by Cambridge University Press

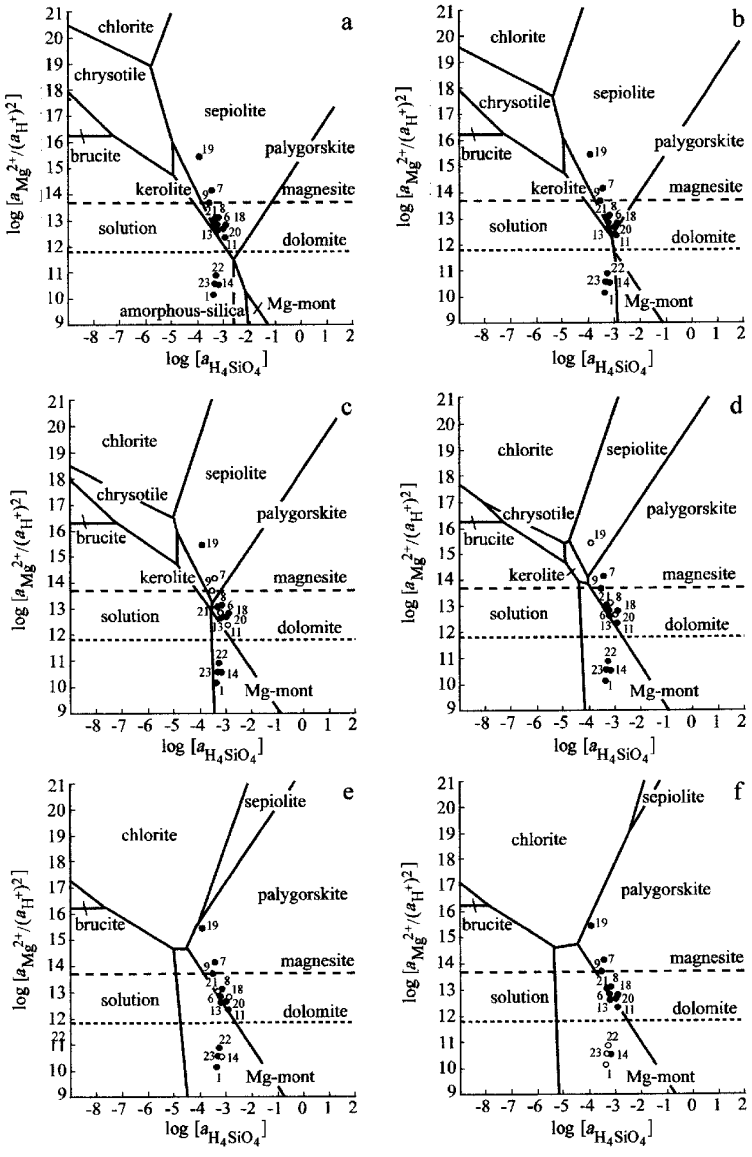

Figure 5. Same as Figure 4 but suppressed with respect to talc, saponite and quartz.

In Figures 3 and 5, amorphous silica is considered to be the controlling silica phase. In this case, the solutions are rich in silica, and palygorskite, sepiolite and amorphous silica can all form. At lower pH values, palygorskite can form through the transformation of the amorphous silica and dioctahedral smectites (Mg-montmorillonite) (Figures 3a and 5a). Palygorskite is also in equilibrium with dolomite. At slightly higher pH values, sepiolite, amorphous silica and palygorskite can form from the solution and also in equilibrium with dolomite. In addition, palygorskite can form from the transformation of dioctahedral smectite and amorphous silica. Occurrences that do not have any amorphous silica or quartz are presented in Figures 3b and 5b. Under this condition, palygorskite can form directly from the solution alone, together with Mg-montmorillonite or from the transformation of Mg-montmorillonite. The behavior of phases in the diagrams of Figures 3d–f and 5d–f are the same as Figures 2d–f and 4d–f.

Plotting the groundwater data of the Amboseli deposit on the activity diagrams (Figures 4 and 5) indicates that the reaction path leads from Mg-montmorillonite, dolomite and palygorskite eventually to sepiolite. At present, water is not in equilibrium with kerolite. This observation, however, may reveal that kerolite is the alteration product of sepiolite, in agreement with the electron microscopy observations of Stoessell and Hay (1978). However, Hay and Stoessell (1984) also showed field evidence for kerolite altering to the sepiolite.

The calculated activity diagrams presented here will provide a rigorous chemical context for field occur-

https://doi.org/10.1346/000986002762090263 Published online by Cambridge University Press

rences. The topologies of the diagrams show that in silica-poor solutions, the formation of sepiolite requires a higher pH than palygorskite, *i.e.* higher silica but lower Al activities encourage sepiolite formation. Palygorskite behaves differently. This observation is supported by experiments showing that palygorskite precipitates over the pH range 7.7–8.5 and sepiolite 8.5–9.5 (Galán and Castillo, 1984). High-silica solutions ($\log[a_{H_4SiO_4}] \geqslant -4.75$) are most favored for the direct precipitation of sepiolite from solution. In particular, the common associations of sepiolite with magnesite, and palygorskite with dolomite or Mg-calcite, correlate very well with the natural occurrences (Stoessell and Hay, 1978; Yalçın and Bozkaya, 1995). Similarly, it has generally been observed that a transformational relationship exists between sepiolite and trioctahedral smectites (Galán and Castillo, 1984), and also palygorskite and dioctahedral smectites (Weaver, 1984). The groundwater data of the Amboseli basin also support those transformational relations between kerolite and sepiolite and the occurrence of dolomite along the reaction path.

ACKNOWLEDGMENTS

Critical reviews, comments and valuable suggestions by referees R.K. Stoessell and P.J. Heaney are gratefully acknowledged. This study was funded by Dokuz Eylül University, AFS project, grant number 0909.97.0603.

REFERENCES

Bowers, T.S., Jackson, K.J. and Helgeson, H.C. (1984) *Equilibrium Activity Diagrams for Coexisting Minerals and Aqueous Solutions at Pressures and Temperatures to 5 kb and 600ºC*. Springer-Verlag, New York, 397 pp.

Bozkaya, Ö. and Yalçın, H. (1993) Hekimhan yöresi sepiyolit-paligorskite grubu kil mineralleri: Mineraloji, jeokimya ve oluşum Pp. 111–126 in: *VI National Clay Symposium, Proceedings*, Bogaziçi University, Istanbul, Turkey.

Chahi, A., Duplay, J. and Lucas, J. (1993) Analyses of palygorskite and associated clays from the Jbel Rhassoul (Morocco): Chemical characteristics and origin of formation. *Clays and Clay Minerals*, **41**, 401–411.

Chen, C.H. (1975) A method for estimation of standard free energies of formation of silicate minerals at 298.15 K. *American Journal of Science*, **275**, 801–817.

Chermak, J.A. and Rimstidt, J.D. (1989) Estimating the thermodynamic properties (ΔG_f^o and ΔH^o_f) of silicate minerals at 298 K from the polyhedral contributions. *American Mineralogist*, **74**, 1023–1031

Christ, C.L., Hostetler, P.B. and Siebert, R.M. (1973) Studies in the system MgO-SiO_2-CO_2-H_2O: III. *American Journal of Science*, **273**, 65–83.

Drever, J.I. (1997) *The Geochemistry of Natural Waters Surface and Groundwater Environments*, 3rd edition, Prentice-Hall Inc., New Jersey, 436 pp.

Ece, Ö. I. and Çoban, F. (1990) Origin and significance of the sepiolite beds and nodules in the Miocene lacustrine basin, Eskişehir, Turkey. Pp. 234–245 in: *International Earth Sciences Congress on Agean Regions Proceedings* **I**, (M.Y. Savaşçın and A.H. Eronat, editors).

Esteoule-Choux, J. (1984) Palygorskite in Tertiary deposits of the Armorican Massif. Pp. 75–84 in: *Palygorskite-Sepiolite, Occurrences, Genesis and Uses* (A. Singer and E. Galán, editors). Developments in Sedimentology, **37**, Elsevier, Amsterdam.

Galán, E. and. Castillo, A. (1984) Sepiolite-Palygorskite in Spanish Tertiary basin: genetical patterns in continental environments. Pp. 87–124 in: *Palygorskite-Sepiolite, Occurrences, Genesis and Uses* (A. Singer and E. Galán, editors). Developments in Sedimentology, **37**, Elsevier, Amsterdam.

Garrels, R.M. and. Christ, C.L. (1965) *Solutions, Minerals, and Equilibria*. Harper and Row, New York, 450 pp.

Gustafsson, J.P. (2001) Modeling the acid-base properties and metal complexation of humic substances with the Stockholm Humic Model. *Journal of Colloid and Interface Science*, **244**, 102–112.

Gustafsson, J.P. (2002) http://www.lwr.kth.se/english/OurSoftware/Vminteq/Index.htm

Hay, R.L. and Stoessell, R.K. (1984) Sepiolite in the Amboseli Basin of Kenya: a new interpretation. Pp. 125–136 in: *Palygorskite-Sepiolite, Occurrences, Genesis and Uses* (A. Singer and E. Galán, editors). Developments in Sedimentology, **37**, Elsevier, Amsterdam.

Helgeson, H.C., Delany, J.M., Nesbitt, H.W. and. Bird, D.K. (1978) Summary and critique of the thermodynamic properties of rock-forming minerals. *American Journal of Science*, **278–A**, 227 pp.

Isphording, W.C. (1984) The clays of Yucatan, Mexico: A contrast in genesis. Pp. 59–73 in: *Palygorskite-Sepiolite, Occurrences, Genesis and Uses* (A. Singer and E. Galán, editors). Developments in Sedimentology, **37**, Elsevier, Amsterdam.

Jones, B.F. (1986) Clay mineral diagenesis in lacustrine sediments. *US Geological Survey Bulletin*, **1578**, 291–300

Jones, B.F and. Galán, E. (1988) Sepiolite and palygorskite. Pp. 631–674 in: *Hydrous Phyllosilicates (Exclusive of Micas)* (S.W. Bailey, editor). Reviews in Mineralogy, **19**. Mineralogical Society of America, Washington, D.C.

Kadir, S. and Baş, H. (1995) Mineralogy of Koyunaǵalı (Mihalıççık-Eskişehir) sepiolite occurrences deposits. Pp. 88–105 in: *VII National Clay Symposium Proceedings*, Hacettepe University, Ankara.

Leguey, S., Vidales, M. and Casas, J. (1984) Diagenetic palygorskite in marginal continental detrital deposits located in the south of the tertiary Duero Basin (Segovia, Spain). Pp. 149–157 in: *Palygorskite-Sepiolite, Occurrences, Genesis and Uses* (A. Singer and E. Galán, editors). Developments in Sedimentology, **37**. Elsevier, Amsterdam.

Long, D.G.F., McDonald, A.M., Facheng, Y., Houjei, L., Zili, Z. and Xu, T. (1997) Palygorskite in palaeosols from the Miocene Xiacaowan Formation of Jiangsu and Anhui Provinces, P.R. China. *Sedimentary Geology,* **112**, 281–295.

Mattigod, S.V. and Sposito, G. (1978) Improved method for estimating the standard free energies for formation (ΔG_f^o 298.15) of smectites. *Geochimica et Cosmochimica Acta*, **42**, 1753–1762

Nordstrom, D.K. and Munoz, J.L. (1985) *Geochemical Thermodynamics*. The Benjamin/Cummings Publishing Co. Inc., Menlo Park, California, 477 pp.

Nriagu, J.O. (1975) Thermochemical approximations for clay minerals. *American Mineralogist*, **60**, 834–839.

Robie, R.A. and Hemingway, B.S. (1995) Thermodynamic Properties of Minerals and Related Substances at 298.15 K and 1 bar (10^5 Pascals) Pressure and Higher Temperature. *US Geological Survey Bulletin*, **2131**, Washington, D.C., 461 pp.

Robie, R.A., Hemingway, B.S. and Fisher, J.R. (1978) Thermodynamic properties of minerals and related substances at 298.15 K and 1 bar (10^5 pascals) pressure and at higher temperatures. *US Geological Survey Bulletin*, **1452**, 456 pp.

Singer, A. and Galán, E., editors (1984) *Palygorskite-Sepiolite,*

Occurrences, Genesis and Uses. Developments in Sedimentology, **37**, Elsevier Amsterdam, 352 pp.

Singer, A. and Norrish, K. (1974) Pedogenic palygorskite occurrences in Australia. *American Mineralogist*, **59**, 508–517.

Stoessell, R.K. (1988) 25ºC and 1 atm dissolution experiments of sepiolite and kerolite. *Geochimica et Cosmochimica Acta*, **52**, 365–374.

Stoessell, R.K. and Hay, R.L., (1978) The geological origin of sepiolite and kerolite at Amboseli, Kenya. *Contributions to Mineralogy and Petrology*, **65**, 255–267.

Tardy, Y. and Duplay, J. (1992) A method of estimating the Gibbs free energies of formation of hydrated and dehydrated clay minerals. *Geochimica et Cosmochimica Acta*, **56**, 3007–3029.

Tardy, Y. and Garrels, R.M. (1974) A method estimating the Gibbs energies of formation of layer silicates. *Geochimica et Cosmochimica Acta,* **38**, 1101–1116.

Velde, B. (1985) *Clay Minerals, A Physico-Chemical Explanation of their Occurrences*. Developments in Sedimentology, **40**, Elsevier, Amsterdam, pp. 225–256.

Wagnam, D.D., Evans, H.E., Parker, V.B., Schumm, R.H., Hallow, I., Bailey, S.M., Churney, K.L. and Nuttall, R.L. (1982) The NBS Tables of Chemical Thermodynamic Properties. *Journal of Physical Chemistry Reference Data*, **11**, National Bureau of Standards Washington, D.C., 393 pp.

Weaver, C.E. (1984) Origin and geologic implications of the palygorskite deposits of SE United States. Pp. 39–58 in: *Palygorskite-Sepiolite, Occurrences, Genesis and Uses* (A. Singer and E. Galán, editors). Developments in Sedimentology, **37**, Elsevier, Amsterdam.

Wollast, R., Mackenzie, F.T. and Bricker, O.P. (1968) Experimental precipitation and genesis of sepiolite at earth-surface conditions. *American Mineralogist*, **53**, 1645–1662.

Yalçın, H. and Bozkaya, Ö. (1995a) Kangal-Çetinkaya alt baseni (SivasBaseni) gölsel paligorskitlerinin mineralojisi ve jeokimyası. Pp. 19–32 in: *VII National Clay Symposium Proceedings,* Hacettepe University, Ankara.

Yalçın, H. and Bozkaya, Ö. (1995b) Sepiolite-Palygorskite from Hekimhan region (Turkey). *Clays and Clay Minerals*, **43**, 705–717.

Yeniyol, M. and Öztunalı, E. (1985) The mineralogy and the genesis of the Yunak sepiolite. Pp. 171–187 in: *II Turkish National Clay Symposium Proceedings*, Hacettepe University, Ankara, Turkey.

(*Received 21 February 2001; revised 9 July 2002; Ms. 525; A.E. Peter J. Heaney*)